J Mater Sci: Mater Electron (2017) 28:4378–4387
DOI 10.1007/s10854-016-6064-2

CrossMark

Studying electrical characteristics of Al_2O_3/PVP nano-hybrid composites as OFET gate dielectric

B. Soltani[1] · M. Babaeipour[1] · A. Bahari[2]

Received: 23 October 2016 / Accepted: 9 November 2016 / Published online: 21 November 2016
© Springer Science+Business Media New York 2016

Abstract Al_2O_3/PVP nano-hybrid composite samples are synthesized using Sol–Gel method at 80 °C. Weight percent of poly 4-vinyl phenol (PVP) and aluminum oxide is 0.0, 0.28, 0.56, and 0.84. To study the nano-structural and electrical characteristics, X-ray diffraction, Fourier transfer infrared radiation, scanning electron microscopy, and atomic force microscopy are used. Dielectric constant of the samples is calculated using GPS 132A technique. The results show that the highest amounts of dielectric constant at the frequency of 120 and 1 kHz are related to Al_2O_3/0.28 wt% PVP (AP 0.28 wt%). PVP ($k = 35$) and Al_2O_3/0.56 wt% PVP (AP 0.56 wt%). PVP ($k = 26$) nano-composite samples, respectively. Therefore, at the frequency of 120 kHz, AP 0.28 wt% PVP nano-composite sample, due to having higher equivalent oxide thickness, less roughness, ohmic properties, smaller size of nano-crystallites (Scherrer diameter of 45 nm), higher dielectric constant, and as a result less leakage current, is recommended as the gate dielectric for the future of organic field effect transistors (OFET).

✉ A. Bahari
a.bahari@umz.ac.ir

M. Babaeipour
babaei@basu.ac.ir

[1] Department of Physics, University of Bu Ali Sina, Hamadan, Iran

[2] Department of Solid State Physics, University of Mazandaran, Babolsar, Iran

1 Introduction

In electronic and nano-optoelectronic devices, particularly in silicon-based field-effect transistors, thickness of gate dielectric reaches about 1–2 nm, which has problems such as increased quantum tunneling, increased leakage current, and boron atom diffusion through the ultra-thin gate dielectric film; consequently, these factors reduce the performance of transistors. Thus, a new architecture is proposed for field-effect transistors [1–9].

In this regard, some researchers have proposed several materials with high dielectric constant, such as Al_2O_3, La_2O_3, HfO_2, Ta_2O_5, TiO_2, and ZrO_2 as the buffer insulator in metal–oxide–semiconductor field-effect transistors (MOSFET) [10–16]. Despite the high rate of dielectric constant, because of the formation of an unwanted intermediate SiO_2 layer between silicon substrate and these materials, they could not replace silicon dioxide as the appropriate gate dielectric [17]. Hence, in recent years, metal oxide and organic matter nano-hybrid composites have been widely welcomed owing to their unique properties in various fields (including catalysts, and electronics) [18–21].

Aluminum oxide, known as alumina, is one of the most important electronic ceramics, which has many industrial applications in micro-electronic industry. Alumina has strong ionic inter-atomic bonds, which is the source of its desirable features. It can exist in different crystalline phases; stable and hexagonal alpha phase at high temperatures is mainly one of the dominant and proposed phases. Because of having a strong and rigid structure, excellent dielectric properties, good thermal properties and strength, and fine aggregate structure, this phase has many applications in electronic devices. Dielectric constant value of alumina is about 9 [22].

On the other hand, due to having different electrical characteristics, organic materials, here, PVP (poly 4-vinyl phenol), have been considered by researchers [23]: superior performance and less cost for processing and construction. Considering the flexibility of its structure, a hybrid of these organic materials has sent a message indicating the establishment of a new space in the field of nano-electronic devices. In this field, composite hybrid of materials such as aluminum oxide and PVP is used to examine the possibility of its introduction instead of silicon oxide. The present research attempts to investigate the nano-structural and electric characteristics of such samples.

2 Experimental procedures

Al_2O_3/PVP nano-hybrid composite samples were synthesized using Sol–Gel method, in which 97% tri-sec-butoxide ($Al[OCH(CH_3)C_2H_5]_3$) with acetylacetone and ethanol solvents as the precursor were used for nano-crystallites. Acetylacetone was used as the PVP solvent; 0.5 ml of tri-sec-butoxide was solved in 5 ml of 98% acetylacetone and 5 ml of 98% ethanol and then was spun on the magnetic stirrer for 2 h at room temperature. At the same time, 0.040 g of PVP was poured into 5 ml of acetylacetone and spun for 2 h on the magnetic stirrer at room temperature until being completely resolved. Then, the second solution was slowly added to the first solution and spun for 22 h on the magnetic stirrer at the room temperature. After this period, the temperature of the magnetic stirrer was adjusted at 150 °C and let it continue spinning. After 2 h, the solution was turned into gel. The gel sample was dried for 15 h in the oven at 70 °C, milled, and turned into a cream-colored smooth powder. Accordingly, AP 0.28 wt% PVP powder sample was achieved. Testing for the weight percentages of 0.56 and 0.84 (0.56 and 0.84 wt%) was also repeated in a completely similar manner and the powders with similar apparent characteristics were obtained. In addition, the test was repeated without PVP (0.00 wt% PVP or 0.00 M PVP).

3 Results and discussion

Many researchers [22–30] have reported that amorphous-shaped gate dielectric, materials with high dielectric constant, low coarseness and surface roughness, high mobility, and low leakage current can be proposed as the candidate for gate dielectric materials. Hence, it is beneficial to ensure that the constructed layers do not have well-defined crystal structures, which is confirmed by XRD results (Philips PW-1710). For this purpose, crystalline phases of nano-hybrid composites are studied by XRD analyses. On the other hand, the performance of OFET devices depends on the use of high-performance dielectrics that form active surfaces, with low defect density or smooth surfaces and good surface topography and morphology. Therefore, microscopic analysis and surface morphology are properly done using SEM and AFM techniques.

Additionally, the correlation between surface roughness and mobility in hybrid composite materials has been recently studied by Chua et al. [29]. They believe that increased surface roughness results in the decreased mobility of OFET. Therefore, it is necessary to study and measure average roughness, average value, and root mean square using Nanosurf software.

Understanding several effective factors in the chemical bonds and bending vibrations of gate dielectric structures is a very important issue. FTIR spectra (Perkin-Element 1730) related to Al_2O_3 powder and Al_2O_3/PVP polymer complexes in terms of transmittance percentage are shown in Fig. 1.

Several peaks are observed in Fig. 1, which are detected using FTIR standard card. FTIR peaks at 690, 580, and 486 cm^{-1} are related to the tensile vibrations of Al–O bond. The presence of peaks at 1596, 1525, and 1394 cm^{-1} are related to the bending vibrations of O–H bond of water adsorption molecules on Al_2O_3. The presence of the flat peak at 3440 cm^{-1} is also related to the tensile vibration of water adsorption molecules on Al_2O_3. As can be seen in this figure, the effect of PVP is revealed as the decreased intensity of the absorption peaks of Al_2O_3. As a result, only through the reduced intensity of the peaks due to the increased PVP weight percent compared with Al_2O_3 substrate, the formation of nano-composite can be confirmed.

Crystalline structures and size of nano-crystallites are determined using X-ray diffraction (XRD). Figure 2 shows the effect of PVP concentration on the diffraction pattern of the studied nano-hybrid composites. By increasing the amount of PVP in the nano-hybrid composites, they are formed in more polycrystalline phases.

As can be observed in Fig. 2a–d, the two presented peaks are related to Al_2O_3 (012) and Al_2O_3 (104) [31]. By increasing the amount of PVP in the powder mixture, no change occurs in Al2O3 phase. But, according to XRD patterns, the intensity of the peaks related to Al_2O_3 (012) and Al_2O_3 (104) is slightly increased and flattened.

Size of crystallite grains is also determined by Scherrer's relation [32].

$$D = \frac{K \cdot \lambda}{\beta \cdot \text{Cos}\theta} \quad (1)$$

where D is average size of Al_2O_3/PVP crystallites, K is Scherrer's constant equal to 0.94, λ is the wavelength of incident radiation ($Cu_{ka} = 1.5406$ Å), β is full width at half maximum (FWHM), and θ is Bragg's angle

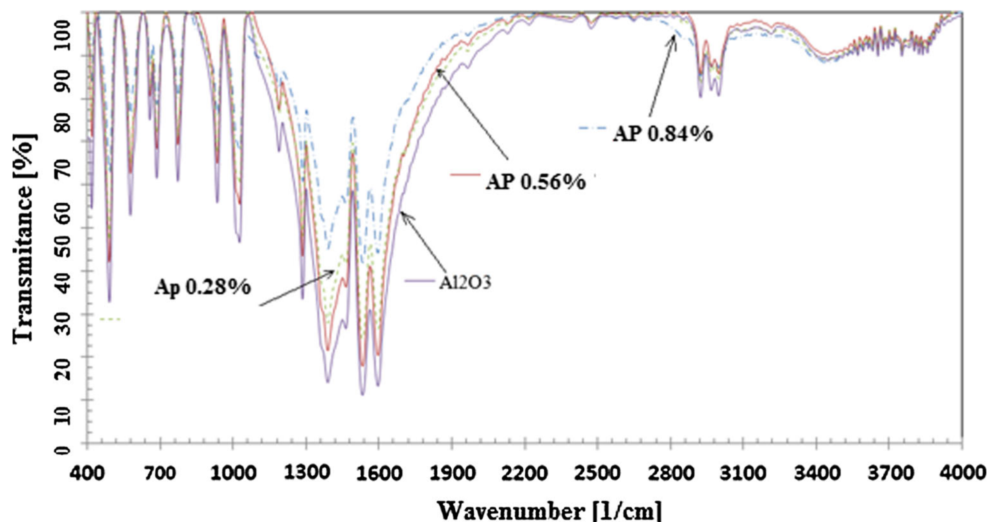

Fig. 1 FTIR spectra of Al_2O_3 and Al_2O_3/PVP (AP) nano hybrid composite with different content of PVP

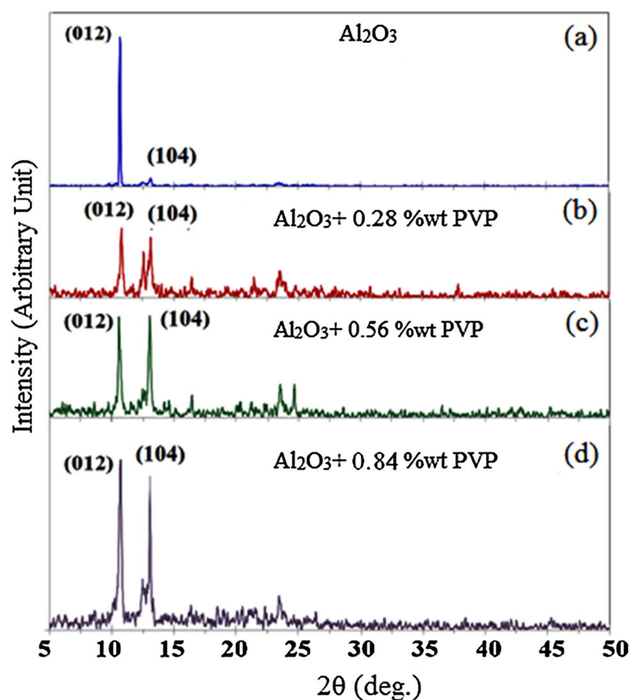

Fig. 2 XRD Patterns of **a** Al_2O_3, **b** AP 0.28 wt% PVP, **c** AP 0.56 wt% PVP, **d** Al_2O_3 + 0.84 wt% PVP nano-hybrid composites. 2θ range 5°–50°

corresponding to the studied peak [33]. In order to calculate the size of crystallites and full width at half maximum (FWHM), X-powder software is used. In Fig. 3, the results of analyzing (012) and (104) peaks in this software are presented. The scheme of the fitted curve and FWHM width is also evident in this figure. Summary results can be found in Table 1, with the explanation that strain is neglected while calculating Scherrer's size.

According to Table 1, minimum size of nano-crystallites using the second and first peaks (104) are related to AP 0.28 wt% PVP (45 nm) and AP 0.84 wt% PVP (62 nm) samples, respectively.

In Fig. 4a–d, EDX analyses obtained from nano-hybrid composites confirm the presence of C, Al, and O nanoparticles. Results of EDX analysis in Table 2 show that the concentration of C is higher in Al_2O_3 + 0.84 wt% PVP sample.

In addition, SEM images of Al_2O_3 samples and different percentages of AP in Fig. 5a–d reveal no obvious crystalline grains, but indicates on signs of brittle fracture on the surface.

According to the SEM images of Al_2O_3 and AP samples, when PVP values increase by 0.28 wt% in Al_2O_3, a smoother surface with less roughness than other PVP values is formed (Table 3). Surface roughness clearly helps increase irregularity and affects the steady growth of semiconductors [34]. It is believed that roughness of the dielectric, due to causing irregularity in the accumulation layer, reduces mobility inorganic semiconductors [29, 35, 36]. As a result, it reduces conductivity as $\sigma = q\left(n\mu_e + p\mu_p\right)$.

Figures 6a–d demonstrate 2D, 3D, and vertical topographic profile of AFM images related to Al_2O_3 and Al_2O_3/PVP nano-hybrid composites with different concentrations of PVP synthesized at 80 °C. In Table 3, roughness factors of Al_2O_3 and Al_2O_3/PVP samples obtained by Nanosurf software are presented [27].

Surface roughness parameters including S_a, S_q, S_m, S_v, S_p, S_y. are also calculated by Nanosurf software.

S_a (average roughness value) is the average sum of the module of distances of all points from the measured surface, in direction, perpendicular to the conditional plane; S_q is root mean square value; S_m (mean roughness value) is also defined by the same average sum, but here the positive or negative values of the vectors are taken into account; S_v

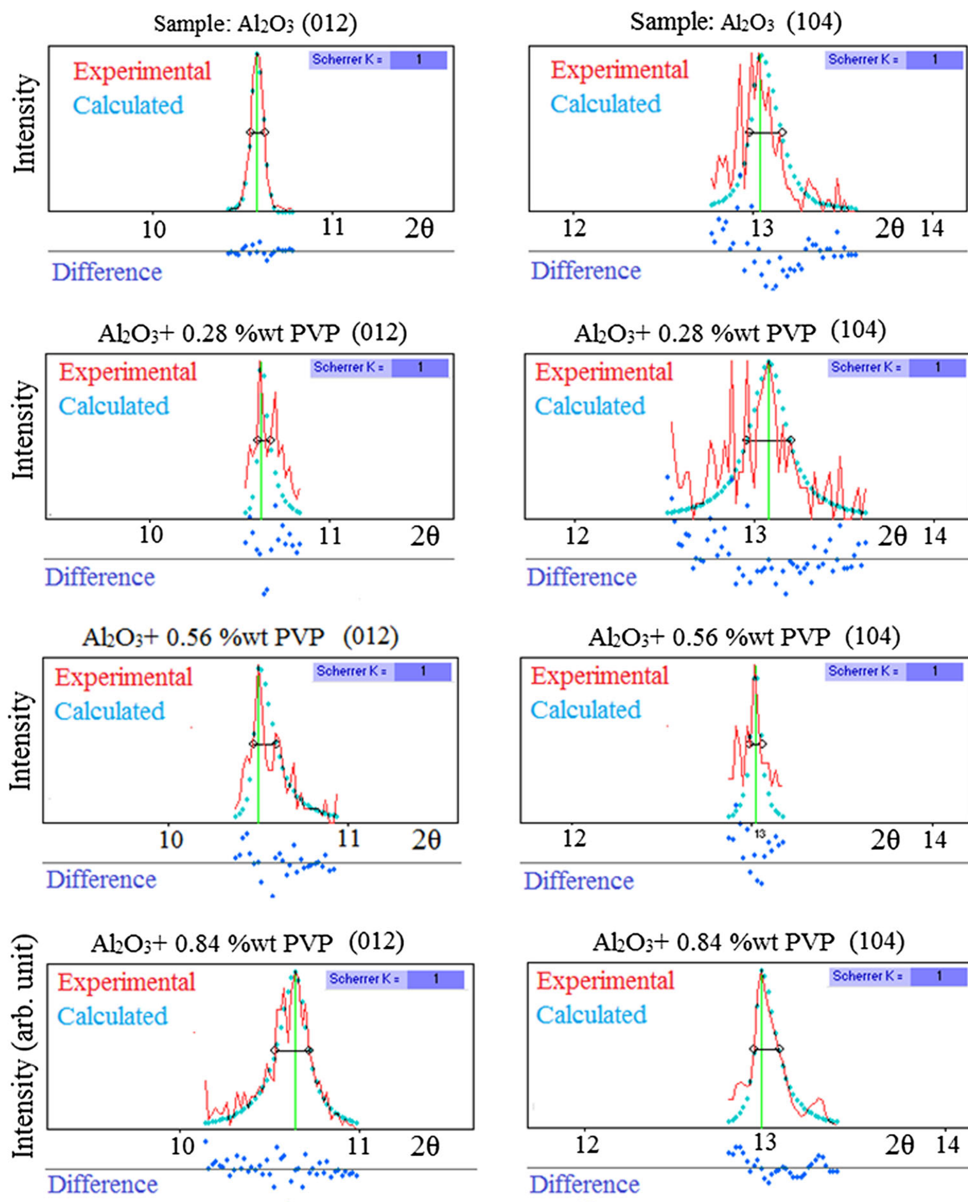

Fig. 3 Calculation of full width at half maximum (FWHM) over the corresponding peaks in XRD patterns for four samples: Al_2O_3, AP 0.28 wt% PVP, AP 0.56 wt% PVP and Al_2O_3 + 0.84 wt% PVP, by using X-Powder software

Table 1 FWHM and Scherrer's crystallite grain size obtained from the (012) and (104) peaks in XRD patterns for four samples: Al_2O_3, AP 0.28 wt% PVP, AP 0.56 wt% PVP and Al_2O_3 + 0.84 wt% PVP, by using X-Powder software

Sample	FWHM		FWHM α_2 corrected		True FWHM		Scherrer (nm)		Corrected Scherrer (nm)	
	(012)	(104)	(012)	(104)	(012)	(104)	(012)	(104)	(012)	(104)
Ap	0.080	0.180	0.073	0.176	0.054	0.129	110	49	163	69
0.28 wt% AP	0.069	0.245	0.060	0.242	0.014	0.195	129	36	634	45
0.56 wt% AP	0.128	0.067	0.124	0.052	0.078	0.006	70	132	114	1576
0.84 wt% PVP	0.190	0.137	0.188	0.132	0.142	0.085	47	65	62	104

Strain is neglected

(valley depth) notes the distance between the conditional plane and the lowest point of the measured surface; S_p (peak height) is the distance between the highest point of the measured surface and the conditional plane; S_y (peak valley height) is the distance between the highest (S_p), and the lowest (S_v) points of the measured surface.

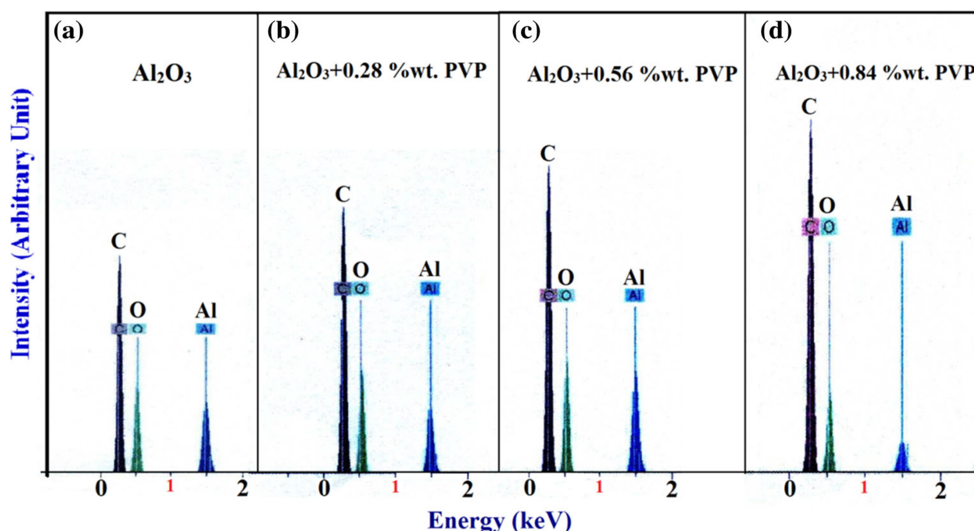

Fig. 4 EDX results for: **a** Al_2O_3, **b** AP 0.28 wt% PVP, **c** AP 0.56 wt% PVP, **d** Al_2O_3 + 0.84 wt% PVP nano hybrid composites

Table 2 EDX results for Al_2O_3, Al_2O_3 + 0.28 wt% PVP, Al_2O_3 + 0.56 wt% PVP and Al_2O_3 + 0.84 wt% PVP Nano hybrid composites

Sample	Series	Norm. C (wt%)			Total (%)	Atom. C (wt%)			Total (%)
		C	O	Al		C	O	Al	
Al_2O_3	K series	48.51	43.57	7.92	100	57.25	38.59	4.16	100
Ap 0.28 wt%	K series	50.52	43.38	6.10	100	58.88	37.96	3.16	100
AP 0.56 wt%	K series	50.06	42.44	7.50	100	58.71	37.37	3.92	100
AP 0.84 wt%	K series	59.07	37.70	3.23	100	66.51	31.87	1.62	100

$$S_a = \frac{1}{MN}\sum_{k=0}^{M-1}\sum_{l=0}^{N-1}|z(x_k, y_l)| \quad (2)$$

$$S_m = \frac{1}{MN}\sum_{k=0}^{M-1}\sum_{l=0}^{N-1}z(x_k, y_l) \quad (3)$$

$$S_q = \sqrt{\frac{1}{MN}\sum_{k=0}^{M-1}\sum_{l=0}^{N-1}(z(x_k, y_l))^2} \quad (4)$$

$$S_v = lowest\ value \quad (5)$$

$$S_p = highest\ value \quad (6)$$

$$S_y = S_p - S_v \quad (7)$$

These parameters are presented in Table 3.

According to the introduced roughness parameters and values obtained in Table 3, S_a, S_q, S_y, S_p values related to AP 0.28 wt% PVP sample are the minimum values which are respectively equal to 16.295, 20.865, 148.13, and 86.875 nm. The minimum difference between peak and valley (S_v) is also related to the same sample. However, as can be seen in the last column of Table 3, S_m value of this sample is the minimum value and equal to 0.3872 pm. Therefore, AP 0.28 wt% PVP sample has the most appropriate surface roughness. Mean fit and Line fit values in Table 4 also confirm the preference of this sample over others.

It is expected from AP nano-hybrid composite with tight surface to have a good blocking function to prevent the growth of the intermediate layer between the gate dielectric and substrate in MOSFETs.

In order to study the electrical properties of the samples, some capacitors are constructed using Al_2O_3 and AP nano-powders, capacity of the samples is measured by PROVA 903 multi-meter, and then dielectric constant (k) is calculated using the equation $k = \frac{cd}{\varepsilon_0 A}$. In the constructed tablets: $A = 1.13cm^2$, $\varepsilon_0 = 8.85 \times 10^{-12}\left(\frac{C^2}{Nm^2}\right)$, and d = 2 mm.

Results in Table 5 show that capacity (C), dielectric constant (k), quality factor (Q_F), and dissipation factor (D_F) change after adding PVP to the samples. The maximum amounts of dielectric constant at the frequency of 1 and 120 kHz are related to Al_2O_3 + 0.28 wt% PVP and Al_2O_3 + 0.56 wt% PVP, respectively.

In Fig. 7, I–V data and the best fitted curves for these data are presented. The comparison between I and V curves shows the differences between Al_2O_3 and AP samples. As can be seen, the relationship between I and V is non-linear (non-ohmic). According to this figure, the curve associated with AP 0.28 wt% PVP sample shows a more ohmic contact behavior than other curves. In Table 6, the characteristics of the fitted curves to data are presented. These curves are exponential and their equation and

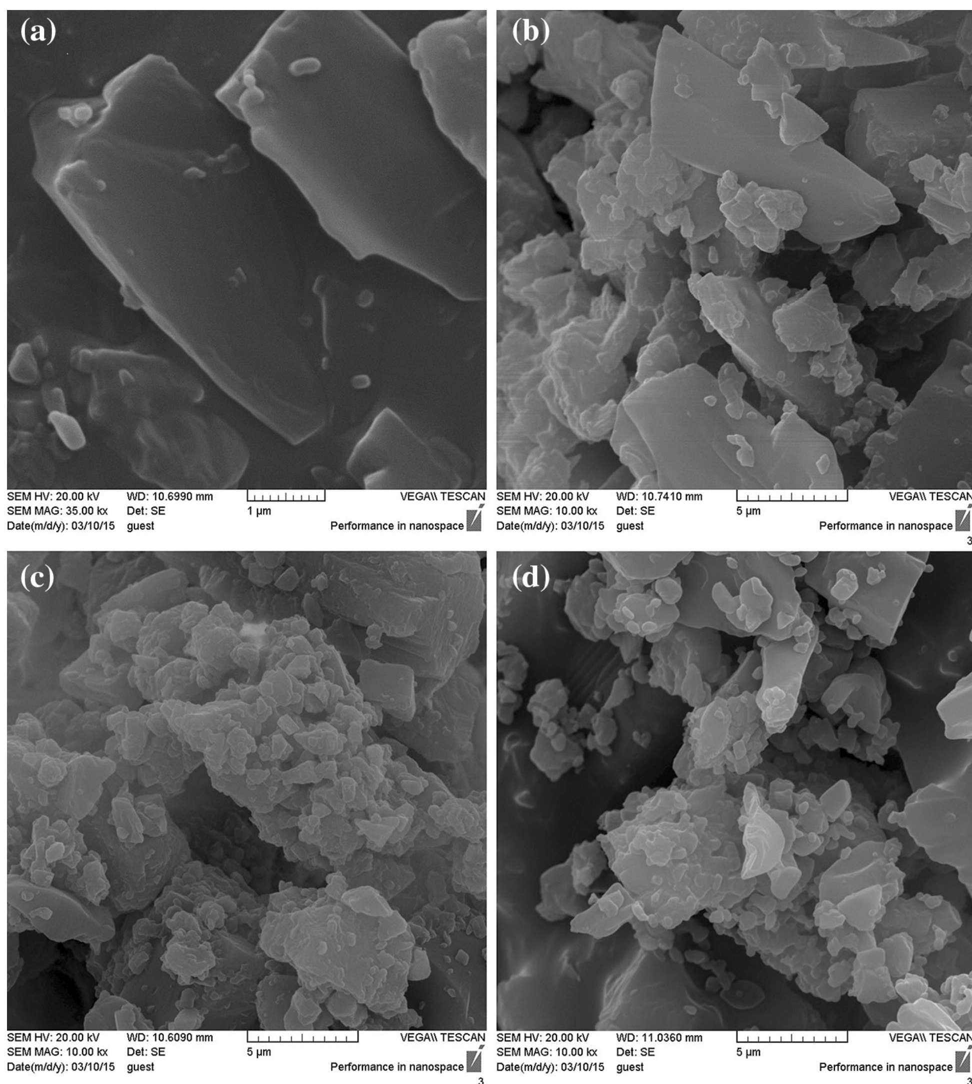

Fig. 5 SEM images of: **a** Al_2O_3, **b** AP 0.28 wt% PVP, **c** AP 0.56 wt% PVP, **d** Al_2O_3 + 0.84 wt% PVP samples

Table 3 Surface roughness factors of Al_2O_3 and AP samples obtained with nanosurf software

Sample	Area (pm^2)	S_a (nm)	S_q (nm)	S_y (nm)	S_p (nm)	S_v (nm)	S_m (pm)
Al_2O_3	9.118	39.121	49.435	319.86	187.92	−131.93	46.02
AP 0.28 wt%	9.118	16.295	20.865	148.13	86.785	−61.34	0.3872
AP 0.56 wt%	9.118	26.677	34.104	245.36	135.79	−109.57	1.0075
AP 0.84 wt%	9.204	21.747	28.495	242.51	127.25	−115.26	24.256

coefficients are presented in the table. Results of goodness of it are given in columns 6 to 9. According to this table, the minimum MSE and RMSE as well as maximum correlation and adjusted R^2 correlation are equal to 10.37, 1.217, 0.999, and 0.9987 and related to AP 0.84 wt% PVP sample, respectively. Goodness of fit values of AP 0.28 wt% PVP sample which are equal to 28.73, 2.026, 0.9971, and 0.9962, respectively, are acceptable values.

The surface under I–V curves related to Al_2O_3/PVP (AP) dielectric nano-crystallites, which can be obtained using cyclic–voltammeter (C–V) technique, is proportional to (P = VI) power. The average amount of current, $\bar{I}$, is obtained as follows:

$$P = \int I dv \tag{8}$$

$$\bar{I} = \frac{P}{\Delta V} \tag{9}$$

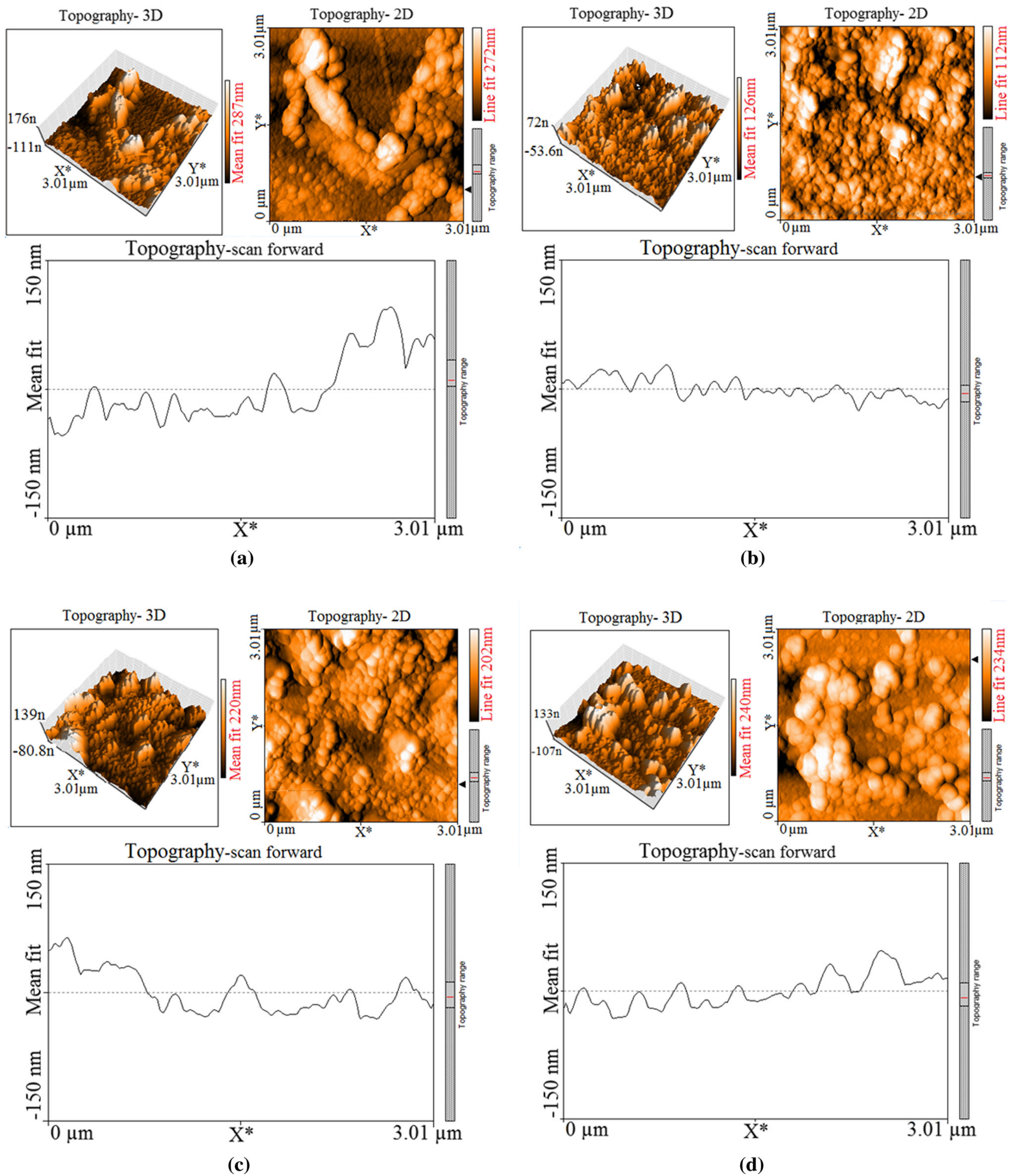

Fig. 6 2D, 3D and best topography profile of **a** Al_2O_3, **b** AP 0.28 wt% PVP, **c** AP 0.56 wt% PVP and **d** Al_2O_3 + 0.84 wt% PVP samples

Higher Q_F value indicates a lower rate of energy loss with respect to stored energy of the capacitor as demonstrated in Eq. (10),

$$Q_F = 2\pi \frac{Energy\,stored}{energy\,dissipated\,per\,cycle} \tag{10}$$

Table 4 Mean fit and line fit for Al_2O_3 and Nano hybrid composite samples AP

Sample	Mean fit (nm)	Line fit (nm)
Al_2O_3	287	272
AP 0.28 wt%	126	112
AP 0.56 wt%	220	202
Al_2O_3 + 0.84 wt%	240	234

D_F value defined with Eq. (11) gives the loss-rate of energy of capacitor and varies with the dielectric material as presented in Table 5.

$$D_F = 1/Q_F \quad (11)$$

Likewise, mathematically, the expression for current density according to Poole–Frenkel model can be written as [37]:

Table 5 C, k, Q_F and D_F of Al_2O_3 and AP obtained by using PROVA 903 multi-meter technique where wafer capacitor surface and wafer thickness are A = 1.13 cm^2 and 2 mm, respectively for frequency = 1 and 120 kHz

Samples	Frequency = 1 kHz				Frequency = 120 kHz			
	Q_F	D_F	C (pF)	k	Q_F	D_F	C (pF)	k
Al_2O_3	26.1	0.038	4.7	14	5.0	0.199	5.0	15
AP 0.28 wt%	3.4	0.298	7.5	15	1.4	0.704	17.0	**35**
AP 0.56 wt%	1.7	0.592	12.9	**26**	5.1	0.198	3.0	6
AP 0.84 wt%	4.8	0.208	6.2	12	2.2	0.457	8.0	16

Bold values indicate high-k material respect to other present samples

C capacity, *k* dielectric constant, *QF* quality factor, *DF* dissipation factor

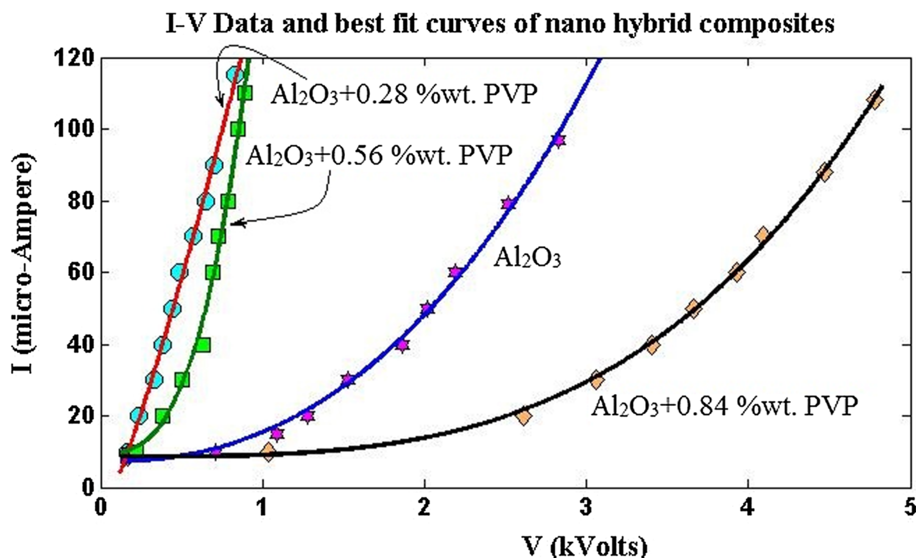

Fig. 7 The I–V data and best fit curves for Al_2O_3, Al_2O_3 + 0.28 wt% PVP, Al_2O_3 + 0.56 wt% PVP and Al_2O_3 + 0.84 wt% PVP samples

Table 6 Fit curve equation coefficients and goodness of fit parameters for Al_2O_3, Al_2O_3 + 0.28 wt% PVP, Al_2O_3 + 0.56 wt% PVP and Al_2O_3 + 0.84 wt% PVP samples

Sample	Fit curve eq.	Coefficients (with 95% confidence bounds)			Goodness of fit			
		a	b	c	SSE	R^2	Adjusted R^2	RMSE
Al_2O_3	$f(x) = a*x^b + c$	8.137	2.329	7.21	109.9	0.9866	0.9849	3.706
AP 0.28 wt%	$f(x) = a*x^b + c$	152.4	1.182	−8.718	28.73	0.9971	0.9962	2.026
AP 0.56 wt%	$f(x) = a*x^b + c$	142.8	2.908	9.435	73.81	0.9926	0.9901	3.57
AP 0.84 wt%	$f(x) = a*x^b + c$	0.5148	3.369	8.545	10.37	0.999	0.9987	1.217

$$J_{PF} = AT^2 exp\left(\frac{1}{K_B T}\left[\left(\frac{57.7eV}{kd}\right)^{\frac{1}{2}} - \varphi_t\right]\right) \tag{12}$$

where k is dielectric constant of the film, d is electrode spacing in A, φ_t is depth of the trap potential well, K_B is Boltzmann constant, T is measurement temperature and A (Richardson constant) is 120 A/cm^2 K^2. Poole–Frenkel effect which has been observed due to trap levels originated from defect levels indicates that adsorbed oxygen atoms present in grain boundary regions can change nano structure as well.

The results show that the maximum value of dielectric constant at the frequency of 1 and 120 kHz is related to AP 0.56 wt% (k = 26) and AP 0.28 wt% (k = 35) nano-hybrid composite samples, respectively (Table 5). This issue indicates the frequency dependence of the dielectric constant caused by the increased tensile vibrations and bond vibrations in the samples. According to Poole–Frenkel effect, these samples have minimum leakage current compared with other samples and can be proposed as a gate dielectric for OFET at the corresponding frequency. In addition, dielectric constant (k) related to SiO_2 and AP 0.28 wt% PVP is respectively equal to k = 3.9 [38] and k = 35. Therefore, according to Eq. (13) and by ignoring φ_t, it can be seen that the leakage current of AP 0.28 wt% PVP sample which is proportional to $exp\left(1/\sqrt{k}\right)$ is decreased greatly compared with silicon dioxide.

$$J_{AP0.28\ wt\%} \propto \exp\left(\left(\frac{1}{k_{AP0.28\ wt\%}}\right)^{1/2}\right) \tag{13}$$

Consequently, the leakage current passing through AP 0.28 wt% PVP sample is significantly reduced.

4 Conclusion

There are several problems that constraint the decreased thickness of gate dielectric. This constraint is caused by boron diffusion from ultra-thin silicon oxide dielectric. A nano-hybrid composite was proposed here to solve this problem. Effective oxide thickness (EOT) of AP 0.28 wt% PVP was 17-fold compared with that of SiO_2, which considerably reduced the leakage current and tunneling current. Therefore, AP 0.28 wt% PVP because of having high dielectric constant and appropriate EOT, minimum roughness, ohmic properties, and small size of nano-crystallites (Scherrer diameter of 45 nm) could be used as a substitute for SiO_2 gate dielectric. Consequently, AP 0.28 wt% PVP nano-hybrid composite could be presented as a possible gate dielectric material for the next generation of OFET devices.

References

1. Y.J. Lee, Formation of aluminum nitride thin films as gate dielectrics on Si (1 0 0). J. Cryst. Growth **266**, 568–572 (2004)
2. A. Bahari, U. Robenhagen, P. Morgen, Z.S. Li, Growth of ultra thin silicon nitride on Si (111) at low temperature. Phys. Rev. B. **72**, 205323–205329 (2005)
3. A. Bahari, P. Morgen, K. Pederson, Z.S. Li, Growth of a stacked silicon nitride/silicon oxide dielectric on Si (100). J. Vac. Sci. Technol., B **24**, 2119–2123 (2006)
4. M. Alagiri, S. Ponnusamy, C. Muthamizhchelvan, Synthesis and characterization of NiO nanoparticles by sol–gel method. J. Mater. Sci.: Mater. Electron. **23**, 728–732 (2012)
5. M. Wu, Y.I. Alivov, H. Moorkoc, High-k dielectrics and advanced channel concepts for Si MOSFET. J. Mater. Sci.: Mater. Electron. **19**, 915–951 (2008)
6. A. Bahari, P. Morgen, K. Pedersen, Z.S. Li, Plasma assisted growth of ultrathin nitrides on Si surfaces under ultrahigh vacuum conditions. J. Phys. Conf. **86**, 012019 (2007)
7. P.R. GiriInt, Atom capture by nanotube and scaling anomaly. J. Theor. Phys. **47**, 1776–1783 (2008)
8. G.D. Wilk, R.M. Wallance, J.M. Anthonyn, High-k gate dielectic current status and material properties considerations. J. Appl. Phys. **89**, 5243–5275 (2001)
9. H. Wu, Y. Zhao, M.H. White, Quantum mechanical modeling of MOSFET gate leakage for high-κ gate dielectric. Solid State Electron. **50**, 1164–1169 (2006)
10. M.G. Blanchin, B. Canut, Y. Lambert, V.S. Teodorescu, M. Zaharescu, Structure and dielectric properties of HfO_2 films prepared by a sol–gel route. J. Sol Gel Sci. Technol. **47**, 165–172 (2008)
11. S. Dell, A. Savin, A. Chadwick, M. Smit, Structural characterization of SiO_2 and Al_2O_3 zener-pinned nanocrystalline TiO_2 by NMR, XRD and electron microscopy. J. Phys. Chem. **111**, 13740–13748 (2007)
12. S.H. Mohamed, M. El-Hagary, A.S. Radwan, Preparation and characterization of mixed iron–titanium oxide nanostructure. Indian J. Phys. **87**, 223–228 (2013)
13. A. Chin, Y. Wu, S. Chen, C. Liao, W. Chen, High quality La_2O_3 and Al_2O_3 gate dielectrics with equivalent oxide thickness 5–10. Technol. Technol. Dig. **16**, 16–17 (2000)
14. S. Zafar, A. Kumar, E. Gusev, E. Cartier, Threshold voltage instabilities in high-κ gate dielectric stacks. IEEE Trans. Dev. Mater. Reliab. **5**, 45–64 (2005)
15. A. Deman, J. Tardy, PMMA-Ta_2O_5 bilayer gate dielectric for low operating voltage organic FETs. Org. Electron. **6**, 78–84 (2005)
16. S.H. Jeong, I.S. Bae, Y.S. Shin, S.B. Lee, H.T. Kwak, J.H. Boo, Physical and electrical properties of ZrO_2 and YSZ high-κ gate dielectric thin films grown by RF magnetron sputtering. Thin Solid Film **475**, 354–358 (2005)
17. B.H. Rudramadevi, K. Thilagavathi, S. Buddhudu, Structural, dielectric and conductivity properties of Mn^{2+}:PVP& Ni^{2+}:PVP polymer films. Indian J. Phys. **86**, 997–1001 (2012)
18. H. Liu, Z.X. Xie, H. Watanabe, J. Qu, K. Tanaka, Growth of nanocrystalline metal dots on the Si(111)-7 × 7 surface saturated with C_2H_5OH. Phys. Rev. B. **601**, 5093–5097 (2007)
19. W.J. Qi, R. Nieh, B.H. Lee, L. Kong, Y. Jeon, K. Onishi, T. Ngai, S. Banerjee, MOSCAP and MOSFET characteristics using ZrO_2 gate dielectric deposited directly on Si. C. Tech. Dig. Int. Electron. Dev. **7**, 145–148 (1999)
20. N. Gang, Y. Wu, B. LiLi, G. Hao, Z. Wenhao, G. Jinzhangl, Preparation of Ps/SiO_2 nanocomposites by surface-initiated nitroxide-mediated radical poly-merization. Chin. Sci. Bull. **51**, 1644–1647 (2006)

21. S. Okur, F. Yakuphanoglu, E. Stathatos, High-mobility pentacene phototransistor with nanostructured SiO_2 gate dielectric synthesized by sol–gel method. Microelectron. Eng. **87**, 635–640 (2010)
22. M. Sonmez, D. Ficai, A. Stan, C. Bleotu, L. Matei, A. Ficai, E. Andronescu, Synthesis and characterization of hybrid PVA/Al_2O_3 thin film. Mater. Lett. **74**, 132–136 (2012)
23. S. Bang, S. Lee, S. Jeon, S. Kwon, W. Jeong, H. Kim, I. Shin, H.J. Chang, H. Park, H. Jeon, Al_2O_3 buffer in a ZnO thin film transistor with poly-4-vinylphenol dielectric
24. M. Shahbazi, A. Bahari, Sh Ghademi, Studying saturation mobility, threshold voltage, and stability of PMMA-SiO_2-TMSPM nano-hybrid as OFET gate dielectric. Synth. Met. **221**, 332–339 (2016)
25. A. Hayati, A. Bahari, Electrical properties of NiO/PVC nano hybrid composites for organic field effect transistors. Indian J. Phys. **89**, 145–154 (2015)
26. A. Bahari, R. Gholipour, Characterization of gate dielectric using high-κ amorphous nanostructures. J. Electron. Mater. (JEMS) **2**, 3529–3540 (2013)
27. X. Peng, G. Horowitz, D. Fichou, F. Garnier, All-organic thin film transistors made of semiconducting alpha-sexithienyl and various polymeric insulating layers. Appl. Phys. Lett. **57**, 2013–2016 (1990)
28. S.H. Kim, W.M. Yun, O.K. Kwon, K. Hong, C. Yang, W.S. Choi, C.E. Park, Hysteresis behaviour of low-voltage organic field-effect transistors employing high dielectric constant polymer gate dielectrics. J. Phys. D Appl. Phys. **43**, 465102 (2010)
29. A. Bahari, M. Roodbari Shahmiri, M. Derakhshi, M. Jamali, Thin film transistors with polyvinylpyrrolidone/nickel oxide sol–gel derived nanocomposite insulator. J. Nanostruct. **2**, 313–316 (2012)
30. L. Chua, P. Ho, H. Sirringhaus, R. Friend, Observation of field-effect transistor behavior at self-organized interfaces. Adv. Mater. **16**, 1609–1615 (2004)
31. A. Bahari, M. Babaeipour, B. Soltani, Theoretical investigation of quantum tunneling and self-energy phenomena in Al_2O_3/PVP nanocomposite. J. Mater. Sci.: Mater. Electron. (JMSE) **27**, 2131–2137 (2016)
32. D. Mohammadiani, S.A. Hosseini, K. Sadrnezhaad, Characterization of nickel oxide nanoparticles synthesized via rapid microwave-assisted route. IJMP: Conf. Ser. **5**, 270–276 (2012)
33. J. Hernandez Torres, A. Mendosa Galven, Formation of NiO–SiO_2 nanocomposites thin films by the sol–gel method. J. Nanocryst. Solids **351**, 2029–2035 (2005)
34. S. Ramesh, K.Y. Ng, Characterization of polymer electrolytes based on high molecularweight PVC and Li_2SO_4. Curr. Appl. Phys. **9**, 329–332 (2009)
35. K.N. Narayanan Unni, S. Dabos-Seignon, J.M. Nunzi, Improved performance of pentacene field-effect transistors using a polyimide gate dielectric layer. J. Mater. Sci. **41**, 317–322 (2006)
36. H. Sirrigahaus, Device physics of solution-processed organic field-effect transistors. Adv. Matter. **17**, 2411–2425 (2005)
37. S.D. Steudel, S.D. Vusser et al., Influence of the dielectric roughness on the performance of pentacene transistors. Appl. Phys. Lett. **85**, 4400–4402 (2004)
38. R.P. Ortiz, A. Facchetti, T.J. Marks, High-κ organic, inorganic, and hybrid dielectrics for low-voltage organic field-effect transistors. Chem. Rev. **110**, 205–239 (2010)